# Blends of the Alternating Ethylene–Tetrafluoroethylene Copolymer with Poly(vinylidene fluoride)

YONGLI MI,[1] JIYUN FENG,[1] CHI-MING CHAN,[1] QIPENG GUO[2]

[1] Department of Chemical Engineering, The Hong Kong University of Science and Technology, Clear Water Bay, Kowloon, Hong Kong

[2] Department of Materials Science and Engineering, University of Science and Technology of China, Hefei 230026, People's Republic of China

*Received 16 September 1996; accepted 16 December 1996*

**ABSTRACT:** Blends of the alternating ethylene–tetrafluoroethylene copolymer (ETFE) with poly(vinylidene fluoride) ($PVF_2$) were prepared by melt-mixing. Compatibility, morphology, thermal behavior, and mechanical properties of the ETFE/$PVF_2$ blends with various compositions were studied by using differential scanning calorimetry (DSC), wide-angle X-ray diffraction (WAXD), dynamic mechanical analysis (DMA), thermogravimetric analysis (TGA), tensile tests, and scanning electron microscopy (SEM). DMA studies showed that the blends have separate glass transition temperatures ($T_g$) close to those of the pure polymers. ETFE and $PVF_2$ are incompatible. Marked negative deviations from simple additivity were observed for both the ultimate strength and the elongation at break over the entire composition range. The interfaces between ETFE and $PVF_2$ are weakly bonded with rather poor interaction. SEM observations revealed that the blends have a two-phase structure and the adhesion between the phases is poor. © 1997 John Wiley & Sons, Inc. J Appl Polym Sci **65:** 295–304, 1997

## INTRODUCTION

Blends of engineering polymers have been under intensive investigation in industrial and academic laboratories for many years because of the strong economic incentives.[1–4] Although it is not always the most efficient, blending is the least expensive and the most versatile technique which can produce new materials from existing commodity polymers. Consequently, their attractiveness increases with the increasing demands for materials of this class.

The alternating ethylene–tetrafluoroethylene copolymer (ETFE) is a high-performance polymer, commercially known as Tefzel of DuPont Co. This polymer shows good mechanical and dielectric properties, good resistance to chemical agents, and good processability.[5] Detailed studies of ETFE have been made in the past few years, including the characterization of its structure and properties as well as pursuing its applications.[6–18] However, to our best knowledge, no work has been done on blends of ETFE with other polymers.

In this contribution, we are concerned with blends of ETFE with another fluoropolymer poly(vinylidene fluoride) ($PVF_2$). $PVF_2$ was chosen as the counterpart polymer because $PVF_2$ and ETFE are isomers. In particular, attention was paid to the compatibility, morphology, and thermal and mechanical properties of these blends. The techniques employed included differential scanning

*Correspondence to:* Y. Mi.

Contract grant sponsor: RGC Earmarked Grants for Research.
Contract grant numbers: 581/94E and 582/95P.
Contract grant sponsor: Chinese Academy of Sciences.
Contract grant sponsor: State Science and Technology Commission of China.
Contract grant sponsor: National Natural Science Foundation of China.
Contract grant number: 59525307.

calorimetry (DSC), wide-angle X-ray diffraction (WAXD), dynamic mechanical analysis (DMA), thermogravimetric analysis (TGA), tensile tests, and scanning electron microscopy (SEM).

## EXPERIMENTAL

### Materials and Preparation of Blends

The alternating ethylene–tetrafluoroethylene copolymer (ETFE) used in this study is Tefzel 200, a commercial product of DuPont Co. The $PVF_2$ is Hylar 460 of Ausimont USA; it has a melt viscosity of 25,500–30,500 poise at 100/s and 232°C.

ETFE/$PVF_2$ blends were prepared by a Haake plasticorder mixer at 300°C for 15 min. The samples were further pressed at 300°C into sheets with thickness of ca. 1.0 mm. Blend compositions studied were 100/0, 90/10, 80/20, 70/30, 60/40, 50/50, 40/60, 30/70 20/80, 10/90, and 0/100 in terms of weight ratios.

### Differential Scanning Calorimetry

A TA 2910 differential scanning calorimeter was employed to study the melting behavior of the samples. The instrument was calibrated with an indium standard. The measurements were conducted under a nitrogen atmosphere. The sample weight used in the DSC cell was kept in the range of 8–12 mg. All samples were first heated to 300°C to remove prior thermal histories. They were then cooled at a rate of 20°C/min to trace the crystallization process, followed by heating to 300°C again at a heating rate of 20°C/min to observe the melting behavior. The heat of fusion was calculated from the melting peak area, and the maximum of the endotherm and the minimum of the exotherm were taken as the melting temperature ($T_m$) and the crystallization temperature ($T_c$), respectively.

### Dynamic Mechanical Analyses

Dynamic mechanical measurements were carried out on a TA DMA 983 dynamic mechanical analyzer. The frequency used was 1.0 Hz and the heating rate 3.0°C/min. Specimen dimension was $1.5 \times 1.0 \times 0.1$ cm.

### Thermogravimetric Analyses

Thermal stability to the blends was assessed with a TA TGA 2950 thermogravimetric analyzer. The sample was first ramped to 100°C and then heated at 10°C/min to 700°C. Measurements were conducted in air.

### Tensile Tests

Tensile tests were carried out on an Instron Model 5567 testing machine at room temperature. Standard dumbbell specimens with a $5.0 \times 1.0 \times 0.1$ cm neck were used. Average values were obtained from at least five successful determinations. Crosshead speed was 5.0 cm/min, corresponding to a relative strain rate of 1.0 $min^{-1}$.

### WAXD Measurements

The WAXD patterns were taken on a Philips PW 1830 diffractometer with CuK$\alpha$ radiation operating at 40 kV and 50 mA at room temperature. The angular scale and recorder reading ($2\theta$) were calibrated to an accuracy of 0.01°. Samples were of uniform thickness and approximately 1 mm thick.

### Morphological Observation

To investigate the morphology and phase structure of the blends, the specimens were fractured under cryogenic conditions using liquid nitrogen. A JEOL 6300F scanning electron microscope (SEM) was used for observation, before which the surfaces were coated with a thin layer of gold of 200 Å.

## RESULTS AND DISCUSSION

### Glass Transition Temperature

Figure 1 shows the dynamic mechanical spectra of the pure polymers and the ETFE/$PVF_2$ blends. The abrupt increases of tan $\delta$ around 150°C for pure $PVF_2$ and the blends are attributable to the melting of crystalline phases of $PVF_2$. For pure $PVF_2$, the tan $\delta$ vs. $T$ curve shows a relaxation peak at −29°C, which is due to its glass transition. For the blends, this maximum of tan $\delta$ is ascribed to the $T_g$ of the $PVF_2$ phase. However, for the blends with ETFE content of 50 wt % or more, it is difficult to discern the $T_g$ of the $PVF_2$ phase from the figure. For the pure ETFE, there exists a maximum at −108°C of the tan $\delta$ vs. temperature curve, responsible for the $T_g$ of the ETFE. It can also be seen from Figure 1 that this maximum is not remarkably changed with $PVF_2$ content in the

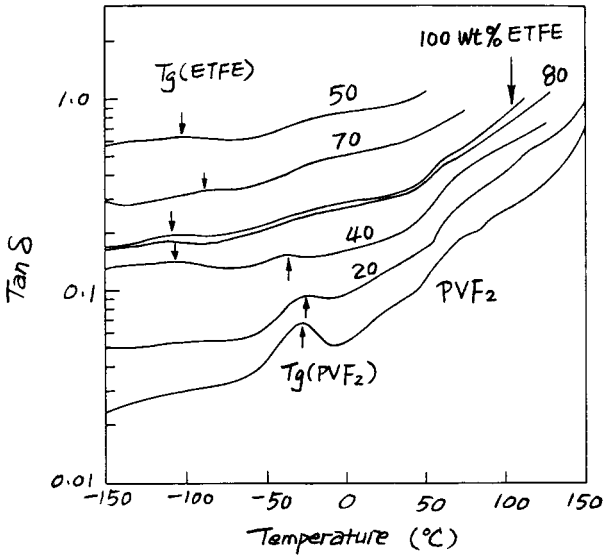


**Figure 1** Tan $\delta$ vs. temperature for the ETFE/$PVF_2$ blends.

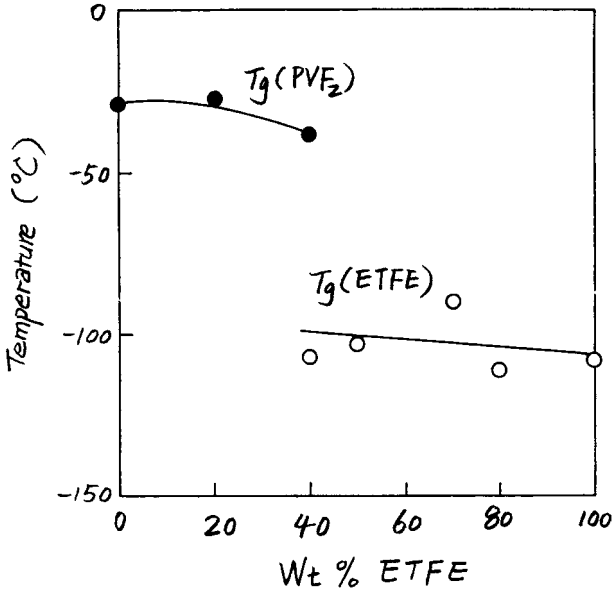


**Figure 2** Glass transition behavior for the ETFE/$PVF_2$ blends obtained by DMA.

blends. The $T_g$ data obtained from Figure 1 are listed in Table I and plotted in Figure 2 as a function of blend composition. Figure 2 clearly displays that the blends have separate glass transition temperatures ($T_g$) close to those of the pure polymers, respectively, although only one $T_g$ was detected at most compositions. It is also noted that the $T_g$ values of both the ETFE and $PVF_2$ phases vary merely within a few degrees with blend composition, implying that these two polymers dissolved little in each other. These results suggest that the ETFE/$PVF_2$ blends are incompatible. It is interesting to see from Figure 1 that abnormal higher values of tan $\delta$ were observed for the blends containing 50 and 70 wt % ETFE, which can be due to the contribution from the loose boundary between the phases particularly observed for these two blends as shown by SEM later.

**Table I $T_g$ Values of ETFE/$PVF_2$ Blends Obtained by DMA**

| ETFE/$PVF_2$ (w/w) | $T_g$ ($PVF_2$) (°C) | $T_g$ (ETFE) (°C) |
|---|---|---|
| 100/0 | | −108 |
| 80/20 | | −111 |
| 70/30 | | −90 |
| 50/50 | | −103 |
| 40/60 | −38 | −107 |
| 20/80 | −27 | |
| 0/100 | −29 | |

## Cooling Crystallization and Melting Behavior

Figure 3 shows the DSC traces of the pure polymers and the ETFE/$PVF_2$ blends at a cooling rate of 20°C/min from 300°C. The related cooling crystallization data are listed in Table II. For the pure $PVF_2$, an exothermic peak occurs at $T_c$ ($PVF_2$) = 126°C. This exothermic peak was observed at the DSC cooling curves for all the blends (Fig. 3). The DSC curves shown in Figure 3 also display the crystallization peaks of the pure ETFE and the blends. In the case of pure ETFE, the cooling crystallization temperature, $T_c$ (ETFE), was observed at 244°C. It is noted that crystallization peaks of ETFE for all the blends keep almost constant. It appears that crystallization of either $PVF_2$ or ETFE was not retarded with the presence of the other component.

Figure 4 summarizes the values of $T_c$ ($PVF_2$) and $T_c$ (ETFE) as functions of blend composition. It can be clearly seen that both the $T_c$ ($PVF_2$) and $T_c$ (ETFE) are invariant with blend composition, indicating that the crystallization rates of both $PVF_2$ and ETFE in the blend are independent of blend composition. This result further shows that $PVF_2$ and ETFE are incompatible.

The melting behavior after cooling from the melt for $PVF_2$, ETFE, and their blends is presented in Figure 5. The DSC curves show separate melting peaks around 167 and 271°C corresponding to $PVF_2$ and ETFE, respectively. A plot of the resulting temperatures (as measured at the tip

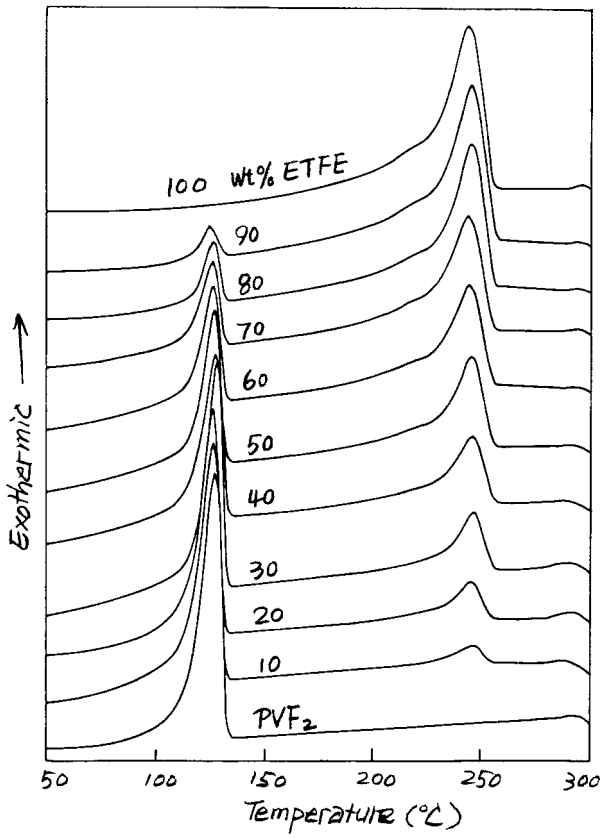


**Figure 3** DSC crystallization curves of ETFE/$PVF_2$ blends during the cooling at 20°C/min.

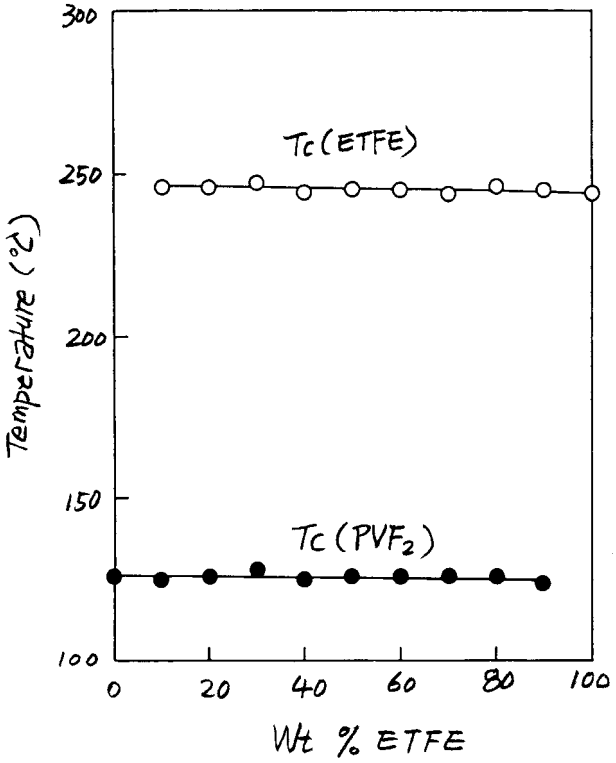


**Figure 4** Composition dependence of nonisothermal crystallization temperatures of ETFE/$PVF_2$ blends.

of the peak) vs. composition for $PVF_2$ and ETFE phases is shown in Figure 6. No depression of the melting temperature of either $PVF_2$ or ETFE associated with the presence of the other component is seen in the figure. By measuring the areas under the melting peaks, it should be possible to evaluate the heat of fusion of each component in the blend. The results so obtained are presented

**Table II Cooling Crystallization Data of ETFE/$PVF_2$ Blends**

| ETFE/$PVF_2$ (w/w) | $\Delta H_c$ ($PVF_2$) (J/g Blend) | $\Delta H_c$ ($PVF_2$) (J/g $PVF_2$) | $T_c$ ($PVF_2$) (°C) | $\Delta H_c$ (ETFE) (J/g Blend) | $\Delta H_c$ (ETFE) (J/g ETFE) | $T_c$ (ETFE) (°C) |
|---|---|---|---|---|---|---|
| 100/0 | | | | 53.0 | 53.0 | 244 |
| 90/10 | 2.9 | 29.0 | 124 | 44.7 | 49.7 | 245 |
| 80/20 | 6.0 | 30.0 | 126 | 40.0 | 50.0 | 246 |
| 70/30 | 10.4 | 34.7 | 126 | 33.1 | 47.3 | 244 |
| 60/40 | 15.0 | 37.5 | 126 | 26.4 | 44.0 | 245 |
| 50/50 | 21.9 | 43.8 | 126 | 23.4 | 46.8 | 245 |
| 40/60 | 24.2 | 40.3 | 125 | 15.2 | 38.0 | 244 |
| 30/70 | 28.5 | 40.7 | 128 | 11.0 | 36.7 | 247 |
| 20/80 | 32.3 | 40.4 | 126 | 6.6 | 33.0 | 246 |
| 10/90 | 37.3 | 41.4 | 125 | 3.0 | 30.0 | 246 |
| 0/100 | 43.3 | 43.3 | 126 | | | |

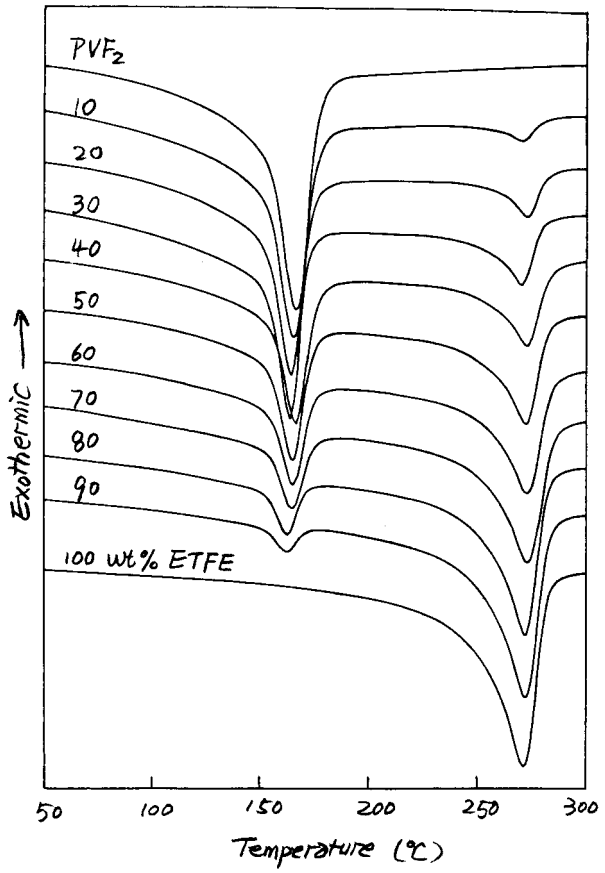


**Figure 5** DSC curves of ETFE/$PVF_2$ blends after the cooling crystallization. The heating rate is 20°C/min.

in Table III. It can be seen that the heat of fusion of either $PVF_2$ or ETFE does not greatly decrease with the presence of the other component. The results presented here further confirm that the $PVF_2$/ETFE blends are incompatible.

### X-ray Diffraction

Figure 7 shows X-ray diffraction diagrams of the pure polymers and the ETFE/$PVF_2$ blends. The WAXD pattern of the pure ETFE gives a single diffraction peak at $2\theta = 19.1°$, which is consistent with the observation by other authors.[6,12,13,19] For the pure $PVF_2$, there exist five diffraction peaks located at $2\theta = 17.7°$, 18.4°, 19.9°, 26.6°, and 33.1° on the WAXD diagram. The X-ray diffraction diagrams in the figure further show that the ETFE/$PVF_2$ blends are all semi-crystalline. However, it is noted that no new diffraction peak was observed for all the blends, indicating that no new crystalline form of either $PVF_2$ or ETFE appeared associated with the presence of the other component. Crystallization of neither $PVF_2$ nor ETFE in the blends was greatly influenced.

### Thermal Stability

To investigate the thermal stability of the blends, TGA was used to measure the degradation process of the blends in air. Figure 8 shows the TGA curves for the ETFE/$PVF_2$ blends with different compositions. It can be seen from the figure that ETFE began to degrade at a lower temperature than $PVF_2$ did. For all the blends, the temperature at which degradation started decreases slightly with increasing ETFE content.

### Tensile Properties

The stress–strain behavior of crystalline polymers was obtained for ETFE and $PVF_2$ and for the blends with $PVF_2$ content up to 30 wt %. The

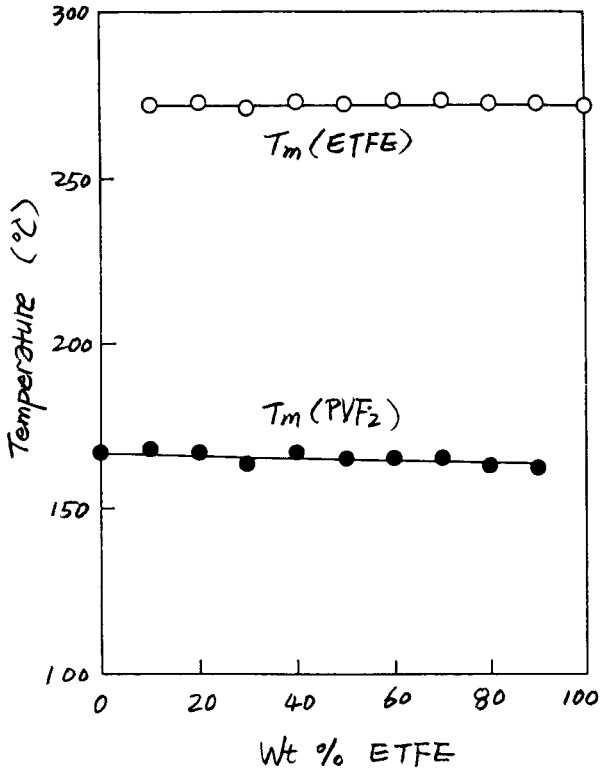


**Figure 6** Variation of the melting temperature of the ETFE/$PVF_2$ blends with composition.

**Table III Melting Behavior of ETFE/$PVF_2$ Blends**

| ETFE/$PVF_2$ (w/w) | $\Delta H_f$ ($PVF_2$) (J/g Blend) | $\Delta H_f$ ($PVF_2$) (J/g $PVF_2$) | $T_m$ ($PVF_2$) (°C) | $\Delta H_f$ (ETFE) (J/g Blend) | $\Delta H_f$ (ETFE) (J/g ETFE) | $T_m$ (ETFE) (°C) |
|---|---|---|---|---|---|---|
| 100/0 | | | | 54.7 | 54.7 | 271 |
| 90/10 | 3.8 | 38.0 | 162 | 47.4 | 52.7 | 272 |
| 80/20 | 7.7 | 38.5 | 163 | 43.1 | 53.9 | 272 |
| 70/30 | 11.8 | 39.3 | 165 | 35.7 | 51.0 | 273 |
| 60/40 | 16.5 | 41.3 | 165 | 28.7 | 47.8 | 273 |
| 50/50 | 21.9 | 43.8 | 165 | 23.6 | 47.2 | 272 |
| 40/60 | 25.0 | 41.7 | 167 | 18.6 | 46.5 | 273 |
| 30/70 | 30.7 | 43.9 | 164 | 12.0 | 40.0 | 271 |
| 20/80 | 36.3 | 45.4 | 167 | 7.2 | 36.0 | 273 |
| 10/90 | 41.8 | 46.4 | 168 | 3.2 | 32.0 | 272 |
| 0/100 | 51.7 | 51.7 | 167 | | | |

stress–strain curve of pure ETFE and pure $PVF_2$ exhibited the characteristics of ductile fracture. However, for the blends with ETFE contents from 10 to 60 wt %, no obvious yield was observed on the stress–strain curves, which shows that these ETFE/$PVF_2$ blends are basically brittle materials at the strain rate of 1.0 $min^{-1}$ and room temperature. From the initial slopes, the Young's moduli of ETFE and $PVF_2$ and of all the blends were calculated. In Figure 9, the Young's modulus is plotted as a function of blend composition. It can be seen that the Young's modulus decreases with increasing ETFE content because of the lower modulus of ETFE.

The properties at high deformation are illustrated in Figures 10 and 11 by their ultimate strength and elongation at break, respectively. Marked negative deviations from simple additivity are observed from the figures for both the ultimate strength and the elongation at break over the entire composition range, which is typical for an essentially incompatible system.[20–25] It may be reasonable to conclude that interfaces between ETFE and $PVF_2$ are weakly bonded with rather poor interaction.

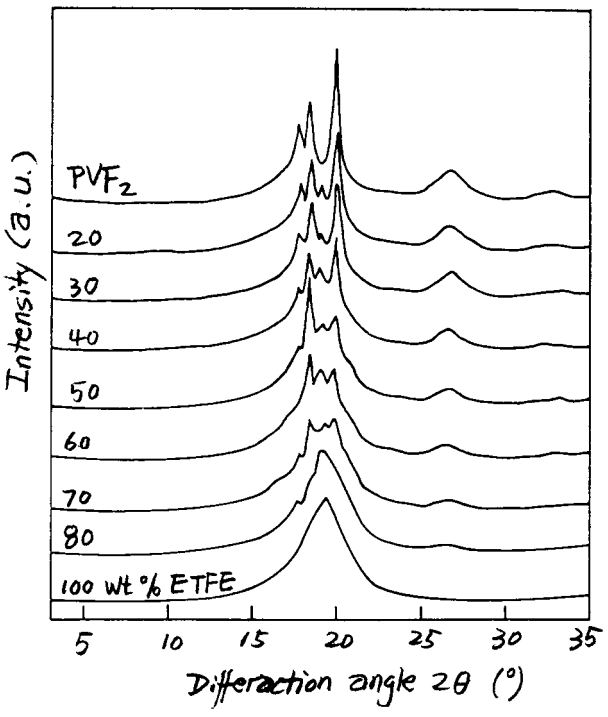


**Figure 7** X-ray diffraction diagram of the ETFE/$PVF_2$ blends.

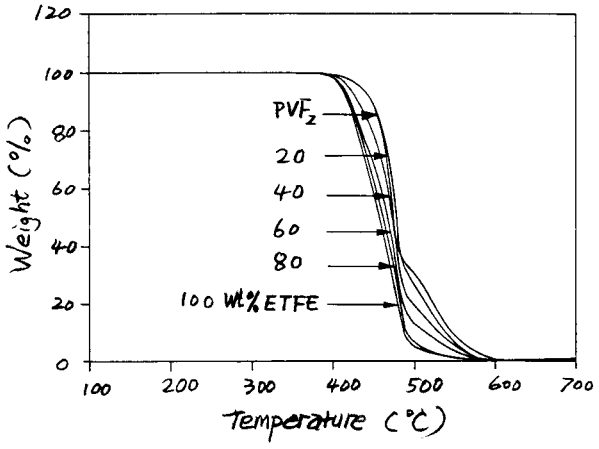


**Figure 8** TGA curves of the ETFE/$PVF_2$ blends heated at 10°C/min in air.

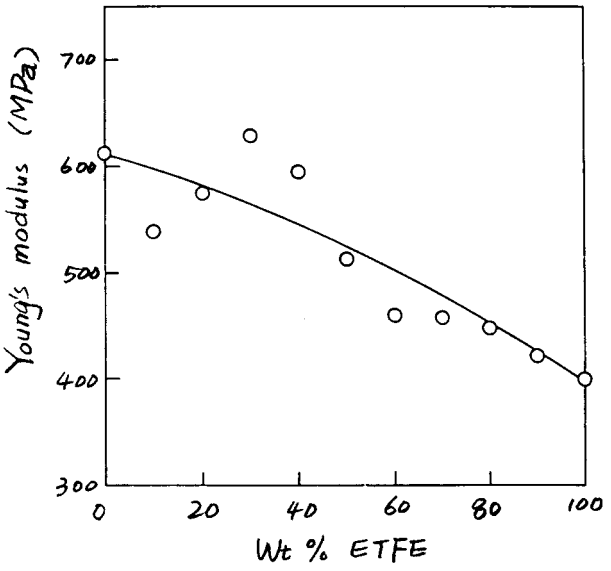


**Figure 9** Composition dependence of the Young's modulus at room temperature for ETFE/$PVF_2$ blends.

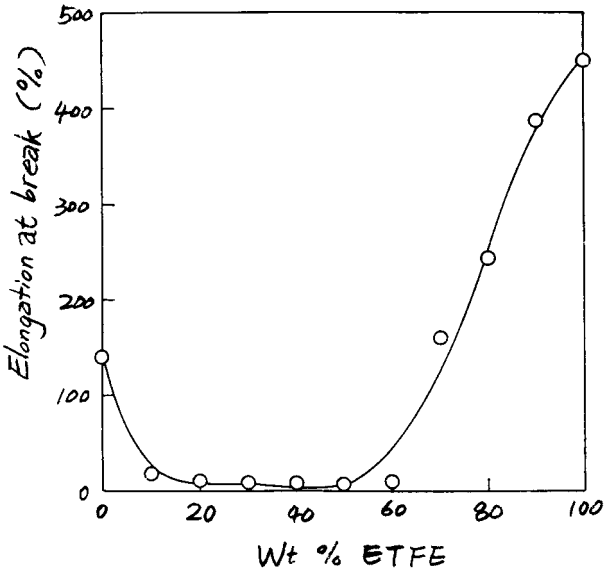


**Figure 11** Composition dependence of elongation at break at room temperature for ETFE/$PVF_2$ blends.

## Morphology

The morphology of the ETFE/$PVF_2$ blends were investigated using scanning electron microscope (SEM). The specimens were fractured under cryogenic conditions using liquid nitrogen. Figure 12 shows the SEM photographs of the fractured surfaces of the blends. They clearly exhibit a two-phase structure of the blends and the poor adhesion between the phases. For the 10/90 and 20/80 ETFE/$PVF_2$ blends, spherical ETFE domains are dispersed in the continuous $PVF_2$ phase [Fig. 12(a) and (b)]. The SEM micrographs also show that there appear vacant holes with regular shapes and broadly distributed sized diameters after the ETFE dispersed phase was pulled off. It can be seen from Figures 12(a) and (b) that the domain sizes of the minor ETFE phase in the 10/90 and 20/80 ETFE/$PVF_2$ blends are in the range from 0.5 to 5 $\mu$m in diameter. Moreover, it is noted that the domain size of the minor ETFE phase increases gradually with ETFE content. For the 30/70 ETFE/$PVF_2$ blend, the dispersed domains of the ETFE phase appear rodlike [Fig. 12(c)]. Furthermore, cocontinuous morphology was observed for the blends with ETFE contents of 50 and 60 wt % [Figs. 12(d) and (e)]. The SEM micrographs of the 70/30 and 90/10 ETFE/$PVF_2$ blends [Figs. 12(f) and (g)] display spherical $PVF_2$ domains dispersed in the continuous ETFE phase. However, the domain sizes of the minor $PVF_2$ phases in the 90/10 and 70/30 ETFE/$PVF_2$ blends are rather large, with a range from 3 to 20 $\mu$m in diameter. It is also interesting to notice from Figure 12 that the domains of minor phases remain intact and the interfaces between ETFE and $PVF_2$ phases are very poorly bonded for all the ETFE/$PVF_2$ blends. Particularly, it is interesting to note from Figures 12(d)–(f) that the

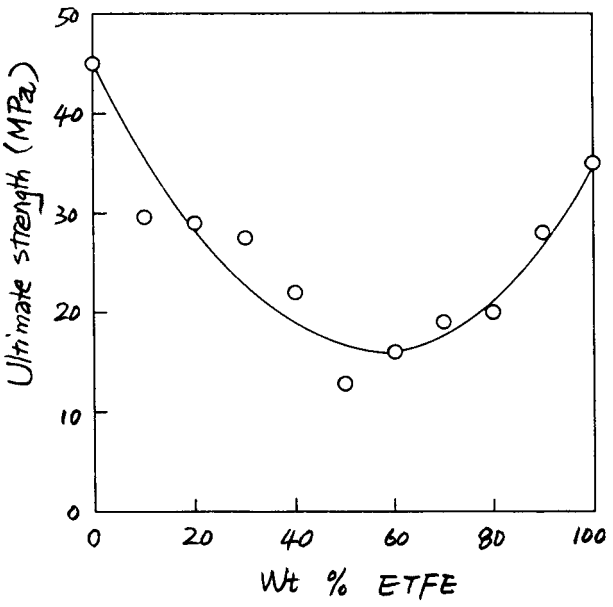


**Figure 10** Composition dependence of ultimate strength at room temperature for ETFE/$PVF_2$ blends.

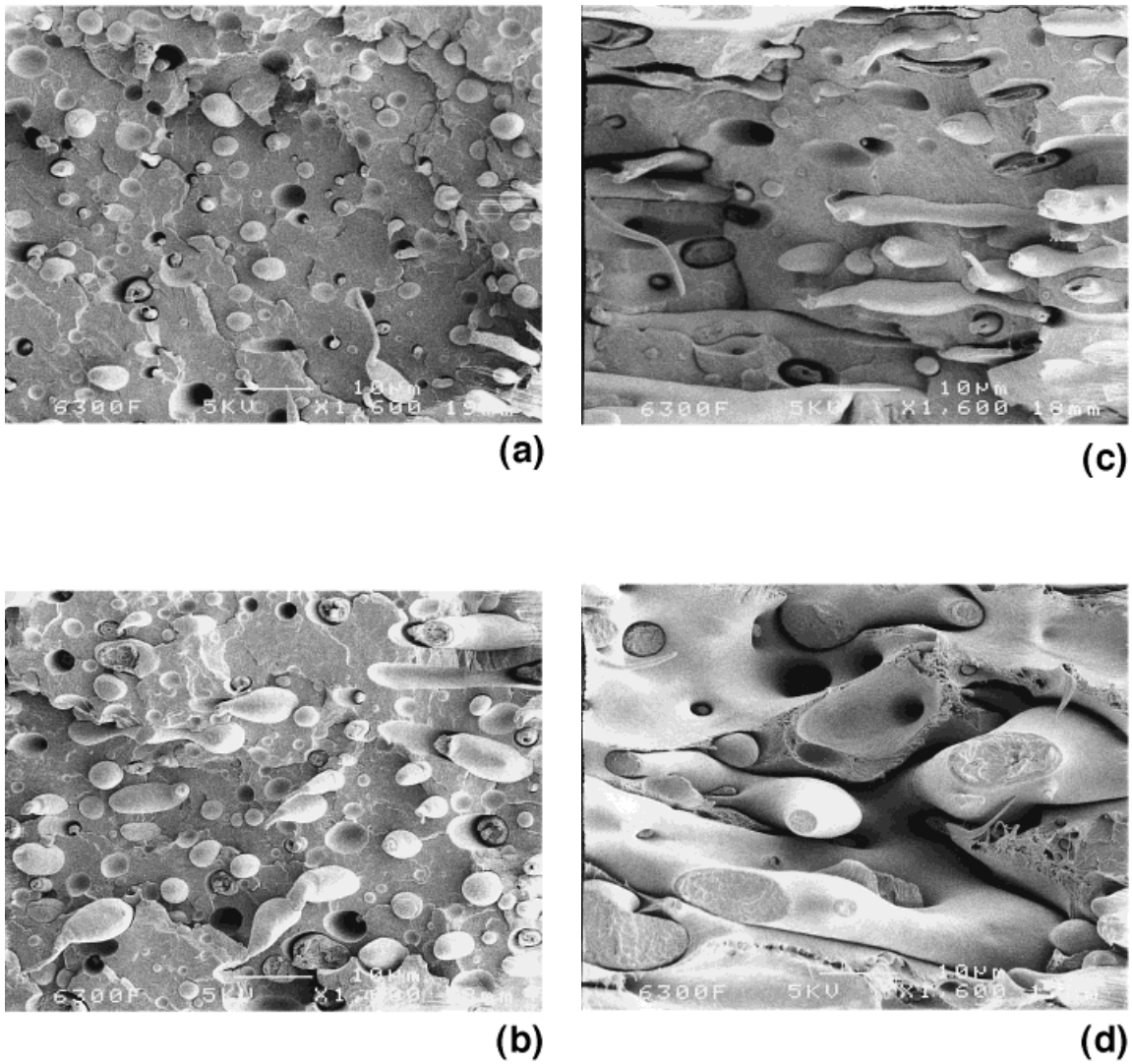


**Figure 12** Scanning electron micrographs of fractured surfaces of the ETFE/$PVF_2$ blends. Blend composition ETFE/$PVF_2$: (a) 10/90; (b) 20/80; (c) 30/70; (d) 50/50; (e) 60/40; (f) 70/30; (g) 90/10.

loose boundary and large size of the phase structure were observed for the blends with ETFE content from 50 to 70 wt %, which is responsible for the abnormal higher values of tan $\delta$ of these blends as mentioned earlier.

## CONCLUSIONS

From the above results it can be concluded that

1. ETFE and $PVF_2$ are incompatible. Their blends have separate $T_g$s close to those of the two pure polymers, respectively.
2. The Young's modulus decreases slightly with increasing ETFE content owing to modulus of ETFE. Marked negative deviations from simple additivity are observed for both the ultimate strength and the elongation at break over the entire composition range, as expected for an essentially incompatible system. The interfaces between ETFE and $PVF_2$ are weakly bonded with rather poor interaction.
3. SEM observations revealed that the blends have a two-phase structure and the adhesion between the phases is very poor.

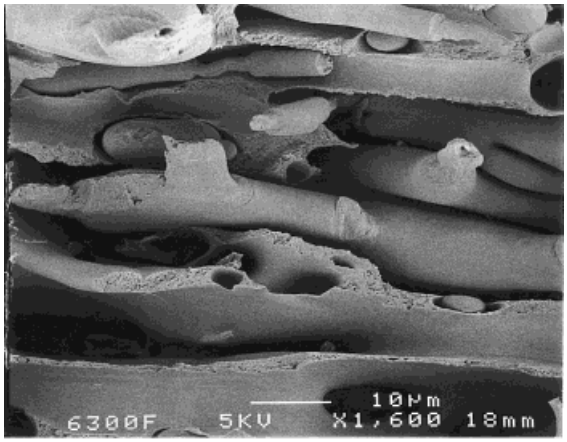


(e)

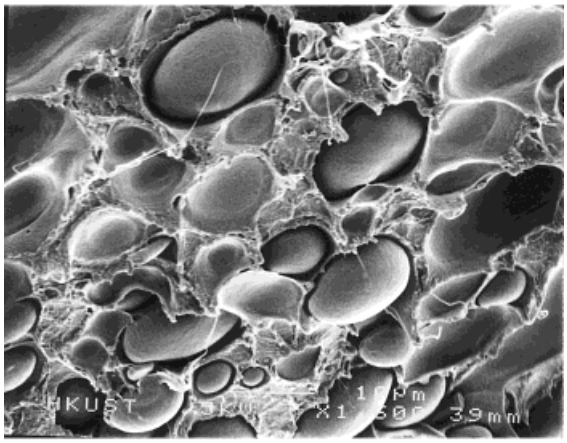


(f)

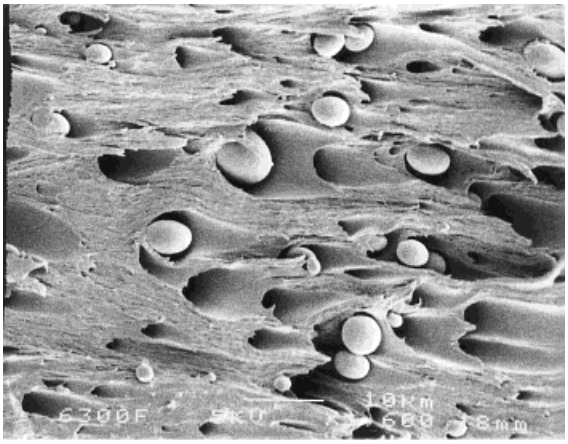

(g)

**Figure 12** (*Continued from the previous page*)

The financial supports of RGC Earmarked Grants for Research (Nos. 581/94E and 582/95P), to this work and to Professor Q. Guo for his visit at HKUST is gratefully acknowledged. One of the authors (Q. G.) is grateful to the Presidential Fund of the Chinese Academy of Sciences and to the State Science and Technology Commission of China for the financial support. He also wishes to express his appreciation to the National Natural Science Foundation of China for awarding a "Premier" Grant for Outstanding Young Scientists (No. 59525307).

## REFERENCES

1. D. R. Paul and S. Newman, Eds., *Polymer Blends,* Academic Press, New York, 1978, Vols. 1 and 2.
2. O. Olabisi, L. M. Robeson, and M. T. Show, *Polymer–Polymer Miscibility,* Academic Press, New York, 1979.
3. L. A. Utracki, *Polymer Alloys and Blends,* Hanser, Munich, 1989.
4. M. M. Coleman, J. F. Graf, and P. C. Painter, *Specific Interaction and Miscibility of Polymer Blends,* Technomic, Lancaster, PA, 1991.
5. G. Ajroldi and P. Pilati, in *Atti del 2° Convegno della Societa Italiana di Reologia,* Siena, Italy, May 10 and 11, 1973.
6. M. Modena, G. Garbuglio, and M. Agazini, *J. Polym. Sci. Polym. Lett. Ed.,* **10,** 153 (1972).
7. L. N. Pirozhnaya and L. I. Tarutina, *Zh. Prikl. Spektros.,* **34,** 862 (1980).
8. A. Dobreva and I. Gutzow, *Cryst. Res. Technol.,* **26,** 863 (1991).
9. A. Dobreva, A. Nikolov, and G. Kostov, *Cryst. Res. Technol.,* **27,** 903 (1992).
10. S. Radce, N. Del Fanti, C. Castiglioni, M. Del Zoppo, and G. Zerbi, *Macromolecules,* **27,** 2194 (1994).
11. F. C. Wilson and H. W. Stakweather, Jr., *J. Polym. Sci. Polym. Phys. Ed.,* **11,** 919 (1973).
12. T. Tanigami, K. Yamaura, S. Matsuzawa, M. Ishikawa, K. Mizoguchi, and K. Miyasaka, *Polymer,* **27,** 999 (1986).
13. T. Tanigami, K. Yamaura, S. Matsuzawa, M. Ishikawa, K. Mizoguchi, and K. Miyasaka, *Polymer,* **27,** 1521 (1986).
14. K. Scheerer and W. Wilke, *Colloid Polym. Sci.,* **265,** 206 (1987).
15. T. Pieper, B. Heise, and W. Wilke, *Polymer,* **30,** 1768 (1989).
16. M. Iuliano, C. De Rosa, G. Guerra, V. Petraccone, and P. Corradini, *Makromol. Chem.,* **190,** 827 (1989).

17. V. Petraccone, C. De Rosa, G. Guerra, M. Iuliano, and P. Corradini, *Polymer,* **33,** 22 (1992).
18. G. Guerra, C. De Rosa, M. Iuliano, V. Petraccone, and P. Corradini, *Makromol. Chem.,* **194,** 389 (1993).
19. C. D'Aniello, C. De Rosa, G. Guerra, V. Petraccone, P. Corradini, and G. Ajroldi, *Polymer,* **36,** 967 (1995).
20. J. Kohler, G. Riess, and A. Banderet, *Eur. Polym. J.,* **4,** 173, 187 (1968).
21. E. H. Merz, G. C. Claver, and M. Baer, *J. Polym. Sci.,* **22,** 325 (1956).
22. J. Periard, A. Banderet, and G. Riess, *Angew. Makromol. Chem.,* **15,** 31, 35 (1971).
23. P. Bataille, S. Boisse, and H. P. Schreiber, *Polym. Eng. Sci.,* **27,** 622 (1987).
24. J. Huang, B. Jiang, and Q. Guo, *Eur. Polym. J.,* **26,** 61 (1990).
25. W. Liu, Q. Guo, and Z. Feng, *J. Appl. Polym. Sci.,* **46,** 1645 (1992).